The 2013 World Congress on
Advances in Structural Engineering and Mechanics (ASEM13)
Jeju, Korea, September 8-12, 2013

Multi-scale overlapping domain decomposition method to consider local effects in the analysis of thin-walled members

*Ashkan Afnani[1)] and R. Emre Erkmen[2)]

[1), 2)] *School of Civil and Environmental Engineering, University of Technology, Sydney, NSW 2007, Australia*
[1)] ashkan.afnaniEsfandabadi@uts.edu.au

ABSTRACT

Thin-walled members are conventionally modeled by one dimensional beam-type finite elements. Due to the rigid cross section assumption in the formulation of this class of elements, only beam-axis-related deformations can be considered, including flexural, tortional and lateral buckling. However, local deformations such as local buckling of web and flanges, which might have significant effects on the global response of the member, are ignored. In order to model these types of deformations shell-type elements are used throughout the domain of the member. While the former lacks accuracy in some cases, the latter creates oversized models that are computationally uneconomical. The purpose of the current study is to develop a multi-scale finite element model to consider the local effects by a multi-scale overlapping decomposition method. In this method, beam-type elements are used as a basis for the whole domain of the member, while shell-type elements are placed in critical regions only to incorporate the local effect on the global behavior. Therefore, it allows considering the local deformations in the numerical analysis without using shell-type elements throughout the domain. The method proposed herein is applicable under loading cases that cause moment gradient. Numerical examples are provided in which the results are compared to the full-shell-type model, indicating the efficiency and accuracy of the proposed technique.

[1)] Graduate Student
[2)] PhD, Lecturer.

1. Introduction

Thin-walled members are extensively used in different types of structures as main or secondary structural elements. Due to their geometrical property (i.e. having one dimension significantly larger than the others) they are mostly modeled by simple beam-type finite elements. However, these types of elements are formulated by rigid cross-section assumption and consequently are not able to consider cross-sectional deformations such as the local buckling in web or flange and distortional buckling. Alternatively, should the cross-sectional deformations be of interest, one has to perform a more complicated shell-type analysis for the whole domain of the structure.

Recent focus of research on computational mechanics has been on adaptive numerical methods such as mechfree methods (e.g. Belytschko et al, 1996; Duarte & Oden, 1996; Liu & Belytschko, 1997; Oden et al., 2006; Erkmen & Bradford, 2011), Generalized FEM (e.g. Babuska & Melenk, 1997; Belytschko et al., 2001; Strouboulis et al., 2001) and Multi-scale methods (Fish et al., 1994; Hughes et al., 1998; Hughes & Sangalli, 2007; Liu et al., 2000; Feyel, 2003; Geers et al., 2010), which allow the implementation of more accurate numerical models only at the regions of interest (i.e. where local deformations exist) while keeping the rest of the domain to be modeled by the simpler models. In various types of problems where deformations of multiple scales exist such as crack propagation (Haidar et al., 2003) or localized damage problems (Mosler, 2005), the multi-scale method have been used. Particularly, the bridging multi-scale which was originally developed to enrich the nodal values of the FEM solution with meshfree solutions (Liu et al., 1997) provides a basis to couple problems based on two different physical assumptions. In other words, it allows the separation of the local analysis, which is based on comparatively sophisticated modelling assumptions, from the global analysis, in which rather simplistic assumptions are implemented. For instance, this method has been used in strain localization problems considering micropolar continuum model with different levels of resolution (Kadowaki & Liu, 2004).The problem of the thin-walled beams is one of the cases which lead to deformations with multiple scales due to the interaction of the local buckling (i.e. cross-sectional/local deformations) and the global buckling modes of the member (Bradford & Hancock, 1984). In order to capture local buckling behaviour, several methodologies have been utilized; namely finite strip formulations (e.g. Bradford, 1992), the generalized beam theory (e.g. Davies and Leach, 1994), and shell-type elements (e.g. Ronagh & Bradford, 1996). Recently, Erkmen (2012) developed a numerical technique based on the bridging multi-scale method to consider the effect of the local deformations on the global behaviour of the thin-walled structure. This method allows the use of different kinematic assumptions in the local and global model. Therefore, simple beam-type numerical models were used to evaluate the global behaviour, and more detailed shell-type models were used in the place of localized behaviour. However, due to the specific decomposition operator used, the use of the method was limited to the cases with uniform internal bending moment. The purpose of the current study is to broaden the use of the method to make it applicable for beams with moment gradient, which is the case in practice. In order to specify the efficiency and accuracy of the method, the results are compared to the beam and full shell-type models.

2. Beam-type analysis

The beam-type analysis, which is used for the analysis of the whole domain, is based on classical thin-walled beam theory. The kinematic assumptions of the theory lead to a strain vector consisting of axial strain due to the bending, membrane and torsional actions, and shear strains resulting from torsion only. The strain components can be written in terms of displacements parallel to $\bar{x}$, $\bar{y}$ and $\bar{z}$ directions, i.e. $\bar{u}(\bar{z})$, $\bar{v}(\bar{z})$ and $\bar{w}(\bar{z})$, respectively, the angle of twist of the cross-section $\bar{\phi}$, and their derivatives. The strain vector is decomposed into linear and nonlinear components, i.e. $\bar{\boldsymbol{\varepsilon}}=\bar{\boldsymbol{\varepsilon}}_L+\bar{\boldsymbol{\varepsilon}}_N$. Each part can be obtained by multiplying the matrix of cross-sectional coordinates $\mathbf{S}$ by linear and nonlinear vectors including displacement components.

$$\bar{\boldsymbol{\varepsilon}}_L=\left\langle \bar{\varepsilon}_L \quad 0 \quad \bar{\gamma}_L \quad 0 \right\rangle^{\mathrm{T}}=\bar{\mathbf{S}}\bar{\boldsymbol{\chi}}_L \ , \tag{1}$$

$$\bar{\boldsymbol{\varepsilon}}_N=\left\langle \bar{\varepsilon}_N \quad 0 \quad \bar{\gamma}_N \quad 0 \right\rangle^{\mathrm{T}}=\mathbf{S}\bar{\boldsymbol{\chi}}_N \ , \tag{2}$$

Where

$$\bar{\mathbf{S}}=\begin{bmatrix} 1 & -\bar{x} & -\bar{y} & -\bar{\omega} & \bar{x}^2+\bar{y}^2 & 0 \\ 0 & 0 & 0 & 0 & 0 & 0 \\ 0 & 0 & 0 & 0 & 0 & -2\bar{r} \\ 0 & 0 & 0 & 0 & 0 & 0 \end{bmatrix} , \tag{3}$$

The vector of linear derivatives of the displacement is

$$\bar{\boldsymbol{\chi}}_L{}^{\mathrm{T}}=\left\langle \bar{w}' \quad \bar{u}'' \quad \bar{v}'' \quad \bar{\phi}'' \quad 0 \quad \bar{\phi}' \right\rangle \ , \tag{4}$$

while the nonlinear displacement vector can be considered as follows based on Trahair (1993)

$$\bar{\boldsymbol{\chi}}_N{}^{\mathrm{T}}=\left\langle \frac{1}{2}\left(\bar{u}'^2+\bar{v}'^2\right)-a_x\bar{v}'\bar{\phi}'+a_y\bar{u}'\bar{\phi}'+\frac{1}{2}\left(a_x{}^2+a_y{}^2\right)\bar{\phi}'^2 \quad \bar{v}''\bar{\phi}+a_x\bar{\phi}'^2 \quad -\bar{u}''\bar{\phi}+a_y\bar{\phi}'^2 \quad 0 \quad \frac{1}{2}\bar{\phi}'^2 \quad 0 \right\rangle \tag{5}$$

In Eq. (3), $\bar{x}$ and $\bar{y}$ denote the coordinates of a point on the cross-section, $\bar{r}$ is the normal distance from the mid-surface and the sectorial coordinate $\bar{\omega}=\int h\mathrm{d}\bar{s}$ has been used, in which h is the normal distance to the tangent of the point on the section contour from the arbitrarily located pole with $\bar{x}$ and $\bar{y}$ coordinates (a_x,a_y).

A finite element is formulated by assuming linear interpolation for $\bar{w}$ and cubic interpolations for $\bar{u},\bar{v}$ and $\bar{\phi}$.

Based on the above mentioned assumptions, the variational formulation can be formed to obtain the equilibrium equation as

$$\delta\bar{\Pi}=\int_L\int_A \delta\bar{\boldsymbol{\varepsilon}}^{\mathrm{T}}\bar{\boldsymbol{\sigma}}\,\mathrm{d}A\,\mathrm{d}\bar{z}-\delta\bar{\mathbf{d}}^{\mathbf{T}}\bar{\mathbf{f}}=0\,, \tag{6}$$

In Eq. (6), A is the cross-sectional area; L is the length of the beam and $\bar{\mathbf{f}}$ is the external load vector. The stress expression can be obtained directly from the strains using the linear stress-strain relationship for an isotropic material. Consequently, the first variation of the strain vector can be written as

$$\delta\bar{\boldsymbol{\varepsilon}}=\bar{\mathbf{S}}\bar{\mathbf{B}}\delta\bar{\mathbf{d}}\,, \tag{7}$$

The incremental equilibrium equations can be obtained by subtracting the virtual work expressions at two neighbouring equilibrium states and then linearising the result by omitting the second- and higher-order terms, i.e.

$$\delta\left(\delta\bar{\Pi}\right)\approx\delta\bar{\mathbf{d}}^{\mathbf{T}}\bar{\mathbf{K}}\delta\bar{\mathbf{d}}-\delta\bar{\mathbf{d}}^{\mathbf{T}}\delta\bar{\mathbf{f}}=0 \tag{8}$$

where $\bar{\mathbf{K}}$ is the stiffness matrix of the global beam model, i.e.

$$\bar{\mathbf{K}}=\int_L\int_A \bar{\mathbf{B}}^{\mathrm{T}}\bar{\mathbf{S}}^{\mathrm{T}}\bar{\mathbf{E}}\bar{\mathbf{S}}\bar{\mathbf{B}}\,\mathrm{d}A\mathrm{d}\bar{z}+\int_L\bar{\mathbf{M}}_{\sigma}\,\mathrm{d}\bar{z}\,, \tag{9}$$

in which $\bar{\mathbf{M}}_{\sigma}\delta\bar{\mathbf{d}}=\delta\bar{\mathbf{B}}^{\mathrm{T}}\int_A\bar{\mathbf{S}}^{\mathrm{T}}\bar{\boldsymbol{\sigma}}\,\mathrm{d}A$.

3. Shell-type analysis

In order to capture the buckling behaviour of the thin-walled member, a four-node shell element with 6 degrees of freedom per node is adopted. In order to satisfy C^1 continuity requirement of Kirchhoff plate theory and avoid shear locking effects, Discrete Kirchhoff Quadrilateral (Batoz & Tahar, 1982) is chosen for the plate component, in which shear deformations effects across the thickness is omitted. For the membrane component, the finite element of Ibrahimbegovic et al. (1990) employing drilling degrees of freedom is adopted herein. Displacement degrees of freedom include bending rotations $\hat{\theta}_x$ and $\hat{\theta}_y$ in local *x*-*z* and *y*-*z* planes, drilling rotation $\hat{\theta}_z$ around *z* direction, deflections $\hat{u}_0$ and $\hat{v}_0$ of the mid-surface in local *x*-*y* plane, and the out of plane deflection $\hat{w}_0$ in local *z* direction (Fig. 1.a)

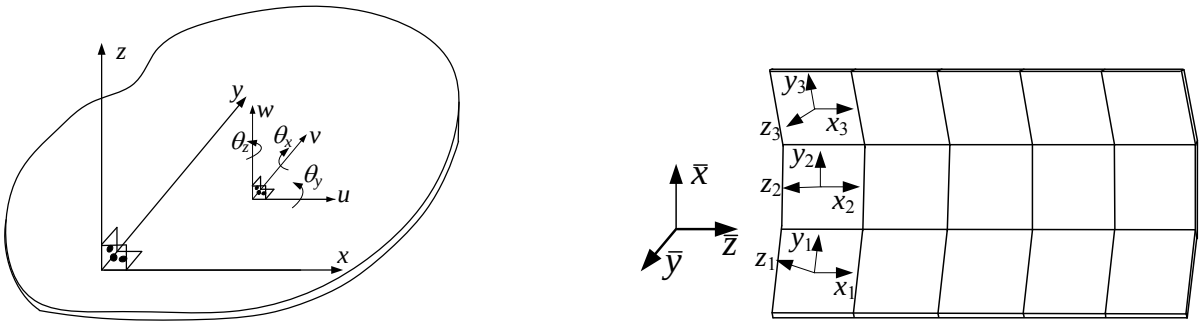

(a) Local deflections of the shell element system

(b) Global vs. local coordinate

Fig.1: Deflections and coordinate systems of the shell formulations

The out of plane deflection $\hat{w}$ is interpolated linearly, while the standard bilinear interpolation is used for the independent drilling rotation $\hat{\theta}_z$, and the Allman-type interpolation functions are used for the in-plane displacements $\hat{u}_0$ and $\hat{v}_0$ (Ibrahimbegovic et al.,1990).The equilibrium equations of the shell model is obtained in the variational form as

$$\delta\hat{\Pi} = \int_L \int_A \delta\hat{\boldsymbol{\varepsilon}}^{\mathrm{T}} \boldsymbol{\sigma} \mathrm{d}A\mathrm{d}\bar{z} - \delta\hat{\mathbf{d}}^{\mathrm{T}}\hat{\mathbf{f}} = 0, \tag{10}$$

$\hat{\boldsymbol{\varepsilon}}$ in Eq. (10) represents the strain vector, which can be composed of strains due to plate bending $\hat{\boldsymbol{\varepsilon}}_b$, membrane action $\hat{\boldsymbol{\varepsilon}}_m$, and strains due to second order membrane and plate bending action $\hat{\boldsymbol{\varepsilon}}_N$, i.e.

$$\hat{\boldsymbol{\varepsilon}} = \boldsymbol{\varepsilon}_b + \hat{\boldsymbol{\varepsilon}}_m + \boldsymbol{\varepsilon}_N \tag{11}$$

where the plate bending strains can be written as

$$\hat{\boldsymbol{\varepsilon}}_b = -z \begin{Bmatrix} \dfrac{\partial \hat{\theta}_x}{\partial x} \\ \dfrac{\partial \hat{\theta}_y}{\partial y} \\ \dfrac{\partial \hat{\theta}_x}{\partial y} + \dfrac{\partial \hat{\theta}_y}{\partial x} \\ \hline 0 \end{Bmatrix} = -z \begin{Bmatrix} \hat{\boldsymbol{\chi}} \\ \hline 0 \end{Bmatrix}, \tag{12}$$

in which $\hat{\boldsymbol{\chi}}$ is the curvature vector. The second term in Eq. (11) can be written as

$$\hat{\boldsymbol{\varepsilon}}_{mm} = \begin{Bmatrix} \dfrac{\partial \hat{u}_0}{\partial x} \\ \dfrac{\partial \hat{v}_0}{\partial y} \\ \dfrac{\partial \hat{u}_0}{\partial y} + \dfrac{\partial v_0}{\partial x} \\ \hline \dfrac{1}{2}\left(\dfrac{\partial \hat{v}_0}{\partial x} - \dfrac{\partial u_0}{\partial y} \right) - \hat{\theta}_z \end{Bmatrix} = \begin{Bmatrix} \hat{\boldsymbol{\varepsilon}}_m \\ \hline \dfrac{1}{2}\left(\dfrac{\partial \hat{v}_0}{\partial x} - \dfrac{\partial u_0}{\partial y} \right) - \hat{\theta}_z \end{Bmatrix}, \tag{13}$$

in which $\hat{\boldsymbol{\varepsilon}}_m$ is the vector of membrane strains and the last row in Eq. (13) contains the skew symmetric part of the membrane strains introduced to avoid numerical stability issues when drilling rotations $\hat{\theta}_z$ are used with Allman-type interpolations. The non-linear strain component can be written as

$$\hat{\boldsymbol{\varepsilon}}_N = \begin{Bmatrix} \dfrac{1}{2}\left(\dfrac{\partial \hat{w}_0}{\partial x} \right)^2 + \dfrac{1}{2}\left(\dfrac{\partial v_0}{\partial x} \right)^2 \\ \dfrac{1}{2}\left(\dfrac{\partial \hat{w}_0}{\partial y} \right)^2 \\ 0 \\ \hline 0 \end{Bmatrix} \tag{14}$$

Similar to the beam model, the equilibrium is obtained by the variational principle as

$$\delta \hat{\Pi} = \int_L \int_A \delta \hat{\boldsymbol{\varepsilon}}^{\mathrm{T}} \boldsymbol{\sigma} \, \mathrm{d}A \mathrm{d}\bar{z} - \delta \hat{\mathbf{d}}^{\mathrm{T}} \hat{\mathbf{f}} = 0 , \tag{15}$$

where $\hat{\boldsymbol{\varepsilon}}$ represents the vector of strain components of the shell element. The potential energy functional is modified according to of Ibrahimbegovic et al. (1990) to prevent numerical stability issues with the Allman type interpolations of the membrane displacements. The stress vector is obtained by assuming linear elastic material.

4. Multi-scale analysis

Fig. 2 shows a schematic of the multi-scale analysis performed. The total domain is shown by Ω_m in the figure, which is modelled by a beam-type finite element. The critical part of the beam – depicted by Ω_c in the figure – is a subset of Ω_m and is modelled by shell elements.

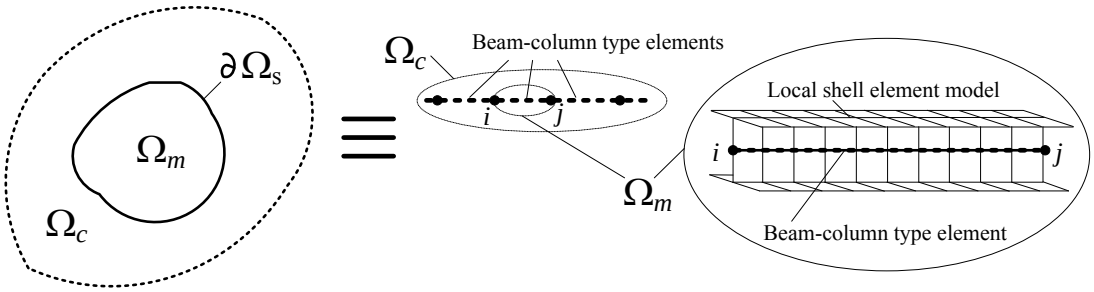

Fig.2: Decomposition of the analysis domain

Based on the Bridging multi-scale approach proposed by Liu et al. (1997, 2003, 2004 and 2006), the shell nodal displacement vector is decomposed into a coarse-scale component and a difference term. To this end, a decomposition matrix N is used, which projects the beam results onto the nodal points of the shell model, i.e. $\hat{\mathbf{d}} = \mathbf{X}\bar{\mathbf{d}} + \mathbf{d}'$, from which the variation of the shell nodal displacement vector can be written as

$$\delta\hat{\mathbf{d}} = \mathbf{N}\delta\bar{\mathbf{d}} + \delta\mathbf{d}', \tag{16}$$

in which the relation $\mathbf{N}\delta\bar{\mathbf{d}} = \mathbf{X}\delta\bar{\mathbf{d}} + \delta\mathbf{X}\bar{\mathbf{d}}$ was used. As a result, the strain vector of the shell model can be decomposed into two parts: $\hat{\boldsymbol{\varepsilon}}=\bar{\boldsymbol{\varepsilon}} + \boldsymbol{\varepsilon}'$, in which the term $\bar{\boldsymbol{\varepsilon}}$ refers to the strain due to the beam formulation. Consequently, the stress vector can be decomposed in the same fashion as $\hat{\boldsymbol{\sigma}} = \bar{\boldsymbol{\sigma}} + \boldsymbol{\sigma}'$. By introducing these values into the variational form of the shell element i.e. Eq. (10), the equilibrium requires the simultaneous satisfaction of the two equations as

$$\delta\Pi_1 = \delta\bar{\mathbf{d}}^{\mathrm{T}}\mathbf{N}^{\mathrm{T}}\int_L\int_A \hat{\mathbf{B}}^{\mathrm{T}}\hat{\mathbf{S}}^{\mathrm{T}}\bar{\boldsymbol{\sigma}}\,\mathrm{d}A\mathrm{d}\bar{z} - \delta\bar{\mathbf{d}}^{\mathrm{T}}\mathbf{N}^{\mathrm{T}}\mathbf{f} + \delta\bar{\mathbf{d}}^{\mathrm{T}}\mathbf{F} = 0\,, \tag{17}$$

and

$$\delta\Pi_2 = \delta\mathbf{d}'^{\mathrm{T}}\int_L\int_A \hat{\mathbf{B}}^{\mathrm{T}}\hat{\mathbf{S}}^{\mathrm{T}}\hat{\boldsymbol{\sigma}}\,\mathrm{d}A\mathrm{d}\bar{z} - \delta\mathbf{d}'^{\mathrm{T}}\,\mathbf{f} = 0\,, \tag{18}$$

The two latter equations are linearized to form the basis for the finite element formulation. The shell solution is obtained by imposing the displacement filed of the

beam element as an interface boundary condition for the shell element. Therefore, the procedure is as follows: firstly, the global problem (i.e. the beam model) is solved to result in the displacement filed $\bar{\mathbf{d}}$ while keeping the fine-scale solution of the local shell model fixed. Then the local model (i.e. the local shell) is solved by imposition of the global displacement as interface boundary conditions to find values of the $\hat{\mathbf{d}}$. Two criteria is checked to ensure the convergence in each load step as suggested by Qian et al (2004) within the framework of Bridging multi-scale method. The first criterion is due to geometric nonlinearity, which confirms that the global equilibrium is achieved at the end of n iterations. Secondly, the difference in the stress vectors of the local shell and the beam model should vanish to ensure that the two solutions are synchronized. In each iteration, the difference between the stress vectors are applied to the model as a complementary force until this force is smaller than a predefined tolerance.

5. Applications

Based on the procedure discussed in previous sections, three numerical experiments are performed to ensure the applicability of the method. In all the cases, the results from the multi-scale procedure are compared with those of the full shell-type model for verification purposes. In order to ensure that the beam-type analysis is kinematically equivalent to the shell model, the comparison with the constraint shell solution is also presented. The constraint shell model is obtained by applying multiple-point constraints on the nodal displacement of the shell model based on the decomposition matric **N,** discussed in section 4.

5.1. Lateral buckling analysis of a simply supported I-beam under moment gradient

A simply supported doubly-symmetric I-beam is analyzed in this section as illustrated in Fig. 3.

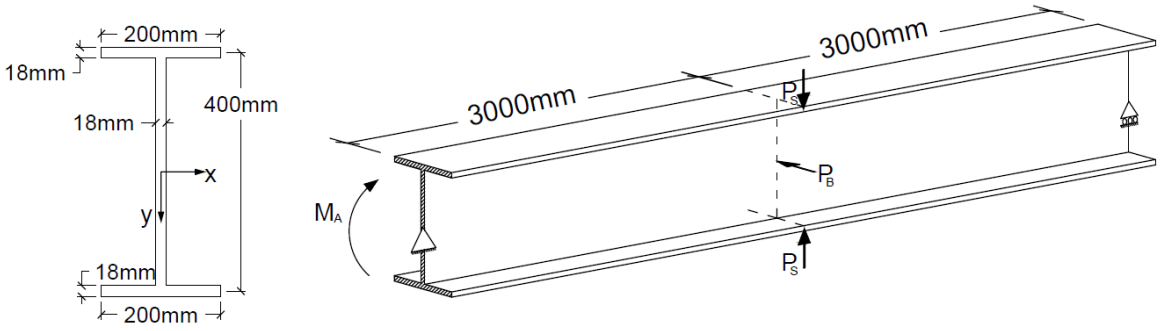

(a) Cross-section (b) Loading and boundary conditions

Fig.3: Cross-sectional and beam geometry of Example 5.1

The cross-sectional dimensions are shown Fig. 3 (a). The beam has a span of $L = 6000mm$ and the material is structural steel $E = 200 \times 10^3$ MPa and $G = 70 \times 10^3$ MPa. For the analysis, beam elements with one meter length are used as the global model, and $200mm \times 200mm$ shell elements are used as the local model. The beam is subjected to a concentrated bending moment at one end, resulting in a linear bending moment gradient. In order to activate the buckling in the nonlinear analysis, a small horizontal load P_B is applied at the mid-span. The load-displacement curves are plotted in Fig. 4 for lateral displacements at the bottom web-flange intersection at mid-span in the absence of a local deformation (i.e., $M_A = 875kNm$, $P_B = 0.1kN$ and $P_S = 0$ in Fig. 3).

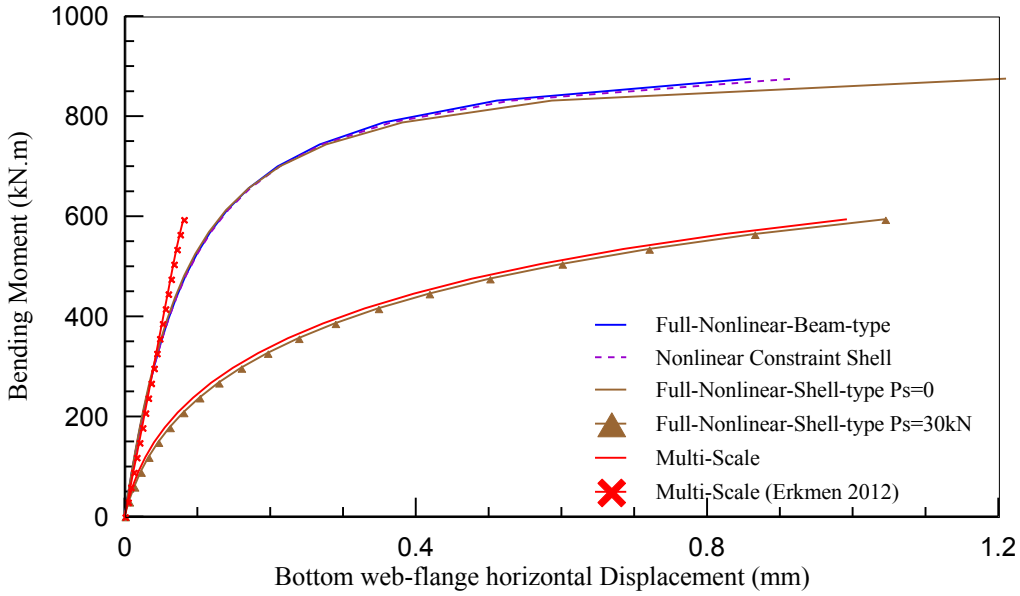

Fig.4: Load-deflection relations based on different modeling types, example 5.1

It can be seen that there is acceptable agreement between the different curves at this stage. Additionally, in order to illustrated the efficiency of the multi-scale approach, local deformations are applied as a force couple at the tip of flanges at the mid-span in addition to the previous loadings (i.e., $M_A = 875kNm$, $P_B = 0.1kN$ and $P_S = 30kN$). The effect of the latter cannot be captured by the global (i.e. beam) model, because the load couple has no resultant at cross-sectional level. Consequently, the results of the beam and the constraint shell model remain constant. However, the load couple has a significant effect on the result of the shell model, which has been accurately captured by the multi-scale model. It should be noted that the overlapping region is from $z = 1400mm$ to $z = 4600mm$, which include approximately half the shell elements used in the full-shell model, indicating the efficiency and the accuracy of the proposed method. It can also be seen that solution in Erkmen [30] cannot accurately capture cases with moment gradient and thus, current modifications are required.

5.2. Lateral buckling analysis of a simply supported I-beam under mid-span load

The same geometry, boundary conditions and material properties as the previous example are used in this model; only the concentrated moment is replaced by a concentrated vertical load at the mid-span. The finite elements used are also identical to the previous case.

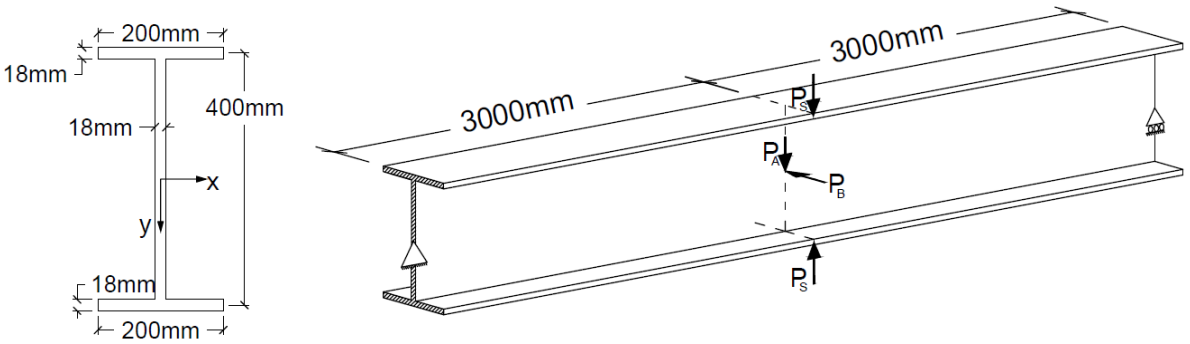

(a) Cross-section (b) Loading and boundary conditions

Fig.5: Cross-sectional and beam geometry of Example 5.2

As in the previous example, the analyses are performed at two stages. Firstly, the vertical point load is applied with a small horizontal load to create small imperfection, (i.e., $P_A = 434kN$, $P_B = 0.1kN$ and $P_S = 0$). Secondly, local deformations are introduced in terms of a load couple of $P_S = 70kN$ with opposite direction at the tip of the flanges at mid-span. As illustrated in Fig. 6, there is a significant softening effect, captured by the shell model, while the beam and the constraint shell remain unchanged. Again it can be observed that by approximately half the shell elements used in the shell model, the multi-scale technique is capable of capturing the behavior accurately. It should be noted that the overlapping region is from z=1400mm to z=4600mm. The answer obtained based on Erkmen [30] is significantly different since the moment gradient effects were not included.

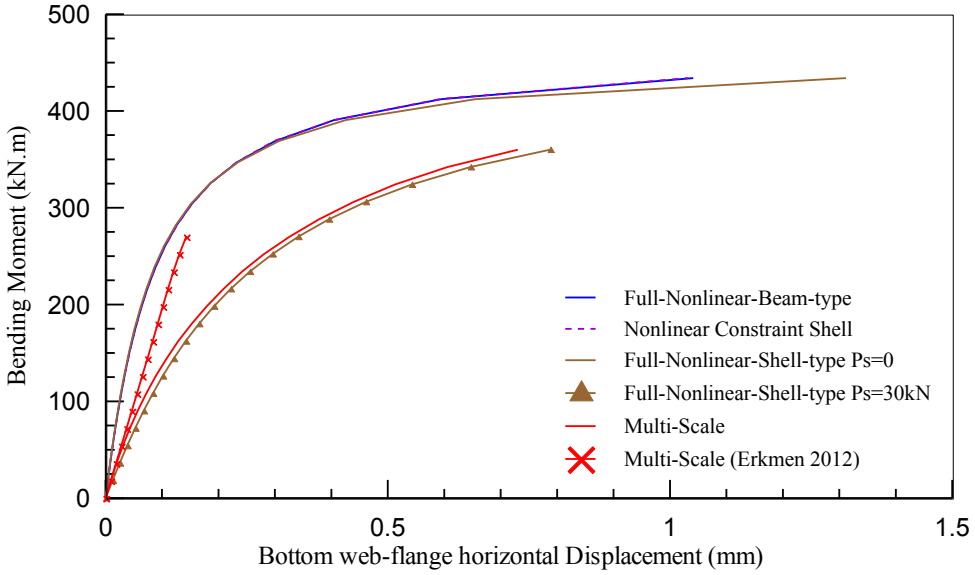

Fig.6: Load-deflection relations based on different modeling types, example 5.2

5.3. Lateral buckling analysis of a continuous beam

In this example a continuous beam with two spans is analyzed, the spans, geometrical and boundary conditions of which is shown in Fig. 7.

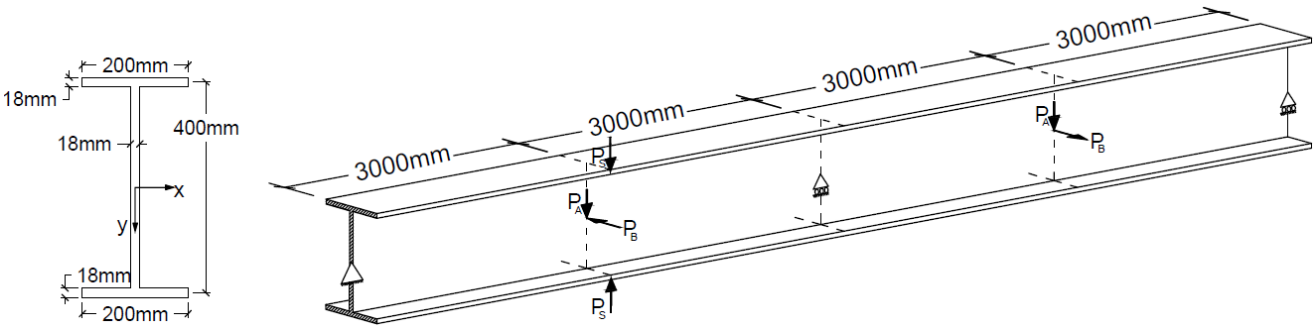

(a) Cross-section (b) Loading and boundary conditions

Fig.7: Cross-sectional and beam geometry of Example 5.3

The material and cross-sectional properties and the finite elements sizes are the same as the previous examples. Two vertical loads are applied at the middle of each of the spans along with two small horizontal loads which act as small imperfection in order to activate the lateral buckling behavior. Similar to the previous examples, the analyses are performed at two stages: Firstly, the results are found according to the

aforementioned loading ($P_A = 742kN$, $P_B = 0.1kN$ and $P_S = 0$). It can be observed from load-deformations curves (Fig. 8) that there is a complete agreement between the beam, shell and constraint shell model at this stage. Secondly, local deformations are introduced in terms of a load couple applied at the tip of the flanges at the middle of one of the spans with a magnitude of 73.75*kN*. Since the load couple have no projection at cross-sectional level, the results of the beam and constraint shell model are not affected by them. On the other hand, the behaviour of the beam changes significantly in the shell solution, which is accurately captured by the multi-scale model according to the load-deformation curves for the first and second span. It should be noted that even though the overlapping region is from z=1400mm to z=4600mm (i.e. at the vicinity of the local deformations only), the behavior is captured accurately at the opposite span (i.e. z=9000mm) as well. This example confirms the efficiency of the multi-scale method, because the effects of the local deformation on the global behaviour is captured accurately by placing approximately ¼ shell elements compared to the full-shell model.

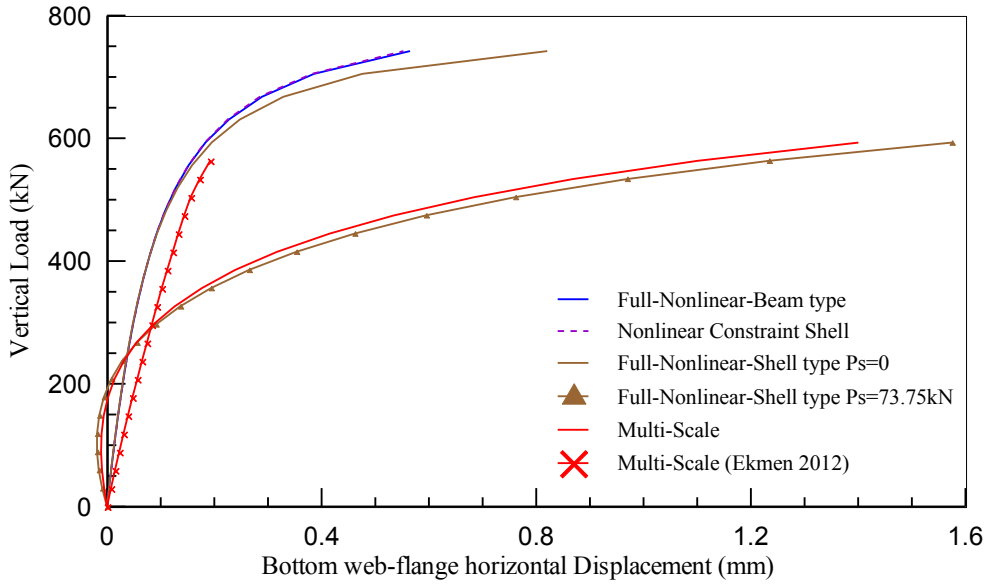

(a) Displacements at Z = 3000mm (the place of local deformations)

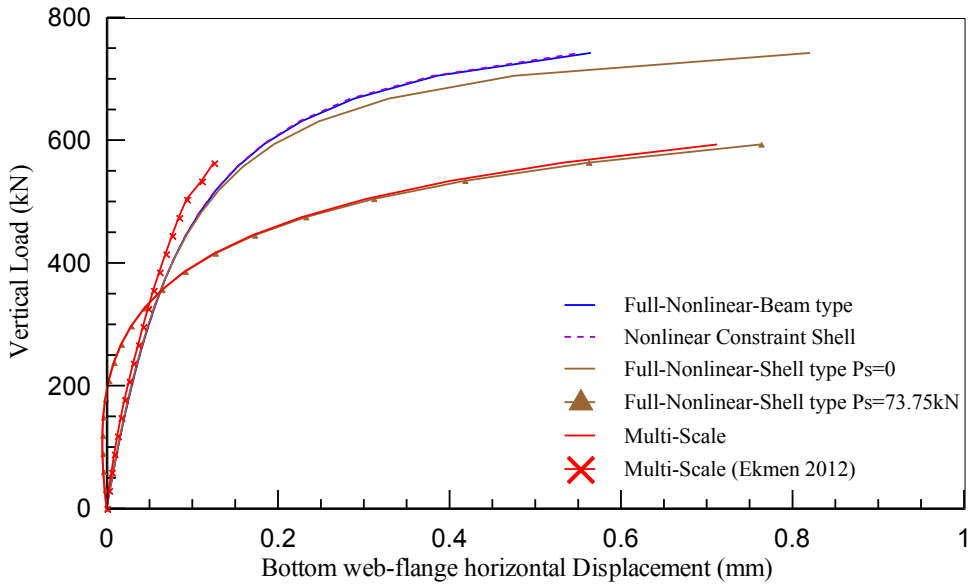

(a) Displacements at Z = 9000mm

Fig.8: Load-deflection relations based on different modeling types, example 5.3

6. Conclusions

In this study, the multi-scale analysis method is developed for the analysis of thin-walled members. The decomposition operator proposed herein can be used to capture the cases under moment gradient effects. It was shown through numerical experiments that the results of the proposed method are accurate, when compared to the full-shell-type model, indicating its accuracy and efficiency.

References

Babuska I, Melenk JM (1997). The partition of unity finite element method. *International Journal for Numerical Methods in Engineering*; 40:727-758.

Batoz J-L, Tahar MB (1982). Evaluation of a new quadrilateral thin plate bending element. *International Journal for Numerical Methods in Engineering*; 18:1655-1677.

Belytschko T, Korungauz Y, Organ D, Fleming M, Krysl P (1996). Meshless methods: An overview and recent developments. *Computer Methods in Applied Mechanics and Engineering*; 139:3-47.

Belytschko T, Moes N, Usui S, Parimi C (2001). Arbitrary discontinuities in finite elements. *International Journal for Numerical Methods in Engineering*; 50:993-1013.

Bradford MA, Hancock G (1984). Elastic interaction of local and lateral buckling in beams. *Thin-walled Structures*; 2:1-25.

Bradford MA (1992). Lateral-distortional buckling of steel I-section members. *Journal of the Constructional Steel Research*; 23:97-116.

Davies JM and Leach P (1994). Second-order generalized beam theory. *Journal of the Constructional Steel Research*; 31:221-241.

Duarte CAM, Oden JT (1996). *Hp* clouds—an *hp* meshless method. *Numerical Methods for Partial Differential Equations*; 12:673-705.

Erkmen RE, Bradford MA (2011). Coupling of finite element and meshfree methods for locking-free analysis of shear deformable beams and plates. *Engineering Computations*; 28: 1003-1027.

Erkmen, R.E. 2012. Bridging multi-scale approach to consider the effects of local deformations in the analysis of Thin-walled members. accepted for publication in *Computational Mechanics*; (16th of September 2012).

Feyel F (2003). A multi-level finite element method to describe the response of highly nonlinear structures using generalized continua. *Computer Methods in Applied Mechanics and Engineering*; 192: 3233-3244.

Fish J, Markolefas S, Guttal R, Nayak P (1994). On adaptive multilevel superposition of finite element meshes for linear elastostatics. *Applied Numerical Mathematics*; 14: 135-164.

Geers MGD, Kouznetsova VG, Brekelmans WAM (2010). Multi-scale computational homogenization: Trends and challenges. *Journal of Computational and Applied Mathematics*; 234: 2175-2182.

Haidar K, Dube, JF, Gilles P-C (2003). Modelling crack propagation in concrete structures with a two scale approach. *International Journal for Numerical and Analytical Methods in Geomechanics*; 45:601-620.

Hughes TJR, Fiejoo G, Mazzei L, Quincy JB (1998). The variational multiscale method- a paradigm for computational mechanics. *Computer Methods in Applied Mechanics and Engineering*; 166: 3-24.

Hughes TJR, Sangalli G (2007). Variational multiscale analysis: The fine-scale Green's function, projection, optimization, localization and stabilized methods. *SIAM Journal of Numerical Analysis*; 45: 539-557.

Ibrahimbegovic A, Taylor RL, Wilson EL (1990). A robust quadrilateral membrane finite element with drilling degrees of freedom. *International Journal for Numerical Methods in Engineering*; 30:445-457.

Kadowaki H, Liu WK (2004). Bridging multi-scale method for localization problems. *Computer Methods in Applied Mechanics and Engineering*; 193: 3267-3302.

Liu WK, Belytschko T (1997). Moving least-square reproducing kernel particle methods (I), Methodology and convergence. *Computer Methods in Applied Mechanics and Engineering*; 143:113-154.

Liu WK, Uras RA, Chen Y (1997). Enrichment of the finite element method with the reproducing kernel particle method. *Journal of Applied Mechanics, ASME*; 64(4):861-870.

Liu WK, Hao S, Belytschko T, Li S, Chang CT (2000). Multi-scale methods. *International Journal for Numerical Methods in Engineering*; 50:993-1013.

Mosler J (2005). On the efficient implementation of an elasto-plastic damage model for large scale analyses of material failure: a multiscale approach. *Computers & Structures*; 83:369-382.

Oden JT, Prudhome S, Romkes A, Bauman PT (2006). Multiscale modelling of physical phenomena: Adaptive control of models. *SIAM Journal on Scientific Computing*; 28: 2359-2389.

Pi Y-L, Bradford MA (2001). Effects of approximations in analyses of beams of open thin-walled sections-part I: Flexural-torsional stability. *International Journal for Numerical Methods in Engineering*; 51: 757-772.

Ronagh HR, Bradford MA (1996). A rational model for distortional buckling of tapered members. *Computer Methods in Applied Mechanics and Engineering*; 130:263-277.

Strouboulis T, Copps K, Babuska I (2001). The generalized finite element method. *Computer Methods in Applied Mechanics and Engineering*; 190: 4081-4193.

Trahair NS. Flexural-Torsional Buckling of Structures. CRC Press, Boca Raton, FL, USA 1993.

Zienkiewics OC, Taylor RL. The finite element method for solid and structural mechanics. Elsevier, sixth edition 2000.